nature communications

Article

https://doi.org/10.1038/s41467-024-52675-x

Annexin A2 promotes proliferative vitreoretinopathy in response to a macrophage inflammatory signal in mice

Received: 18 May 2023

Accepted: 13 September 2024

Published online: 09 October 2024

Check for updates

Min Luo[1], Dena Almeida[1], Valentina Dallacasagrande[1], Nadia Hedhli[1,3], Mrinali Gupta[2], Donald J. D'Amico[2], Szilárd Kiss[2] & Katherine A. Hajjar[1]

Proliferative vitreoretinopathy is a vision-threatening response to penetrating ocular injury, for which there is no satisfactory treatment. In this disorder, retinal pigment epithelial cells, abandon their attachment to Bruch's membrane on the scleral side of the retina, transform into motile fibroblast-like cells, and migrate through the retinal wound to the vitreal surface of the retina, where they secrete membrane-forming proteins. Annexin A2 is a calcium-regulated protein that, in complex with S100A10, assembles plasmin-forming proteins at cell surfaces. Here, we show that, in proliferative vitreoretinopathy, recruitment of macrophages and directed migration of retinal pigment epithelial cells are annexin A2-dependent, and stimulated by macrophage inflammatory protein-1α/β. These factors induce translocation of annexin A2 to the cell surface, thus enabling retinal pigment epithelial cell migration following injury; our studies reveal further that treatment of mice with intraocular antibody to either annexin A2 or macrophage inflammatory protein dampens the development of proliferative vitreoretinopathy in mice.

Proliferative vitreoretinopathy (PVR) is a chronic, fibrosing response to retinal injury[1–4]. A common cause of post-traumatic blindness, PVR occurs in 40–60% of patients with penetrating globe injury, 5–10% of patients with rhegmatogenous retinal detachment[5], and 16–41% of individuals with giant retinal tear[1–4]. While the detailed pathobiology is poorly understood, most authors agree that the development of PVR requires a breach of the blood-retinal barrier and release of circulating blood cells into the injured retina[2,6]. Macrophages that differentiate from blood-derived monocytes, possibly together with local hypoxia, are thought to induce retinal pigment epithelial (RPE) cells to abandon their attachment to Bruch's membrane, proliferate, migrate, and synthesize collagens and other matrix proteins in a process akin to epithelial-mesenchymal transition (EMT)[7–11]. In addition, Müller cells, like other glial cell subpopulations, are activated in response to retinal injury, migrate to the outer nuclear and plexiform layers, and extend processes into the subretinal space[12]. Once formed, PVR membranes can contract, thereby inducing tractional retinal detachment and loss of vision. PVR has increased recently in frequency as a consequence of delays in treatment of retinal detachment due to lockdowns associated with the recent SARS-CoV-2 pandemic[13]. Nevertheless, current treatment for PVR remains unsatisfactory[5,14–16].

Annexin A2 (A2) is a calcium-sensing, phospholipid-binding protein that is expressed as a cytoplasmic monomer and on cell surfaces in a heterotetrameric complex with its binding partner S100A10. The $(A2\text{-}S100A10)_2$ complex is found on endothelial cells, macrophages, glial cells, and RPE cells, as well as a range of other cell types, and binds components of the fibrinolytic plasmin-generating system, namely tissue plasminogen activator (tPA) and plasminogen. Assembly of tPA and plasminogen on the complex accelerates activation of plasmin[17–19], the primary fibrin-clearing protease and a major activator of matrix metalloproteinases[20]. Translocation of intracellular A2 to the cell surface requires the presence of S100A10 as well as Src kinase-mediated phosphorylation of A2. Stimuli, such as thermal stress, thrombin, and glutamate, induce phosphorylation of A2 at tyrosine 23 and enable its

[1]Department of Pediatrics, Weill Cornell Medicine, New York, NY, USA. [2]Department of Ophthalmology, Weill Cornell Medicine, New York, NY, USA. [3]Present address: Hudson Community College, Jersey City, NJ, USA. e-mail: khajjar@med.cornell.edu

translocation, in complex with its binding partner S100A10, from the cytoplasm to the cell surface[21–23]. We showed previously that A2-mediated plasmin activation promotes endothelial cell migration during hypoxic neoangiogenesis[24], supports epithelial-mesenchymal-like transition in the developing avian heart[25], and mediates directed migration of monocytes and macrophages in vitro[18].

Here, we show that annexin A2-deficient mice are resistant to the development of PVR. *Anxa2*$^{-/-}$ mice display minimal histologic alterations associated with PVR in a dispase-induced model. We demonstrate that recruitment of bone marrow-derived macrophage-like cells is inhibited in *Anxa2*$^{-/-}$ mice and that delamination of RPE cells is also minimized. We identify macrophage inflammatory protein-1α (MIP-1α) and MIP-1β as key chemokines that induce Src-mediated tyrosine phosphorylation of A2, thus enabling translocation of A2 to the RPE cell surface. Our studies reveal that treatment of mice with either anti-A2 or anti-MIP-1α/β antibody curtails the development of PVR.

Results

Annexin A2 is Required for Development of PVR

For the present studies, we adapted the standard intravitreal dispase injection model of PVR for use in *Anxa2*$^{+/+}$ and *Anxa2*$^{-/-}$ mice[26–28]. We examined hematoxylin and eosin (H&E)-stained sections through the injection sites of eyes harvested at 6 weeks after dispase administration. In *Anxa2*$^{+/+}$ mice, we noted streaming of RPE cells through the retinal injection wound and incipient formation of an epiretinal membrane within 2 weeks (Fig. 1a, b). By four weeks the normal retinal architecture became distorted and we observed thickening of the epiretinal membrane (Fig. 1e, f). At six weeks, there was often severe distortion of retinal cell layers and complete detachment and contraction of the retina with formation of a dense retrolental mass containing large numbers of pigmented cells and fibroblastoid elements (Fig. 1i, j). In *Anxa2*$^{-/-}$ mice, on the other hand, dispase injection induced only minor distortion of the retinal architecture, minimal RPE cell migration, and no retinal scar formation (Fig. 1c, d, g, h, k, l).

A validated histopathologic scoring system (Suppl. Figure 1a) revealed significantly greater retinal detachment, cellular disorganization, and epiretinal membrane formation in *Anxa2*$^{+/+}$, compared with *Anxa2*$^{-/-}$ in retinas at 2, 4, and 6, weeks post injection ($p = 0.000$-0.0043; Fig. 1m). Similarly, quantification of RPE cell migration resulted in scores that were significantly lower in *Anxa2*$^{-/-}$ versus *Anxa2*$^{+/+}$ eyes ($p = 0.0000$-0.0146; Fig. 1n; Suppl. Figure 1b). In mice receiving a 10-fold lower dose of dispase, moreover, we were unable to appreciate any migration of RPE cells into the injured retina in *Anxa2*$^{-/-}$ eyes, whereas, in *Anxa2*$^{+/+}$ eyes, RPE cells were found streaming through the wound and over the surface of the retina by 4 weeks (Suppl. Figure 2). In addition, to verify that A2 could be central to PVR-like processes in human eyes, we studied human epiretinal membranes removed at surgery. Immunohistologic analysis of 4 out of 4 samples revealed the presence of numerous pigment granule-containing cells (Fig. 2a, b), and costaining of populations of cells positive for CD68 and A2 (Fig. 2c), as well as RPE65 and A2 (Fig. 2d), suggesting that A2-expressing macrophage- and RPE-like cells are present in epiretinal membranes in humans.

We used immunofluorescence staining of mouse retinas to further evaluate early cellular changes in the PVR process (Fig. 3). Within 2 weeks of dispase injection, we noted extensive infiltration of presumptive macrophages that were A2- (green) and CD68-positive (red), in *Anxa2*$^{+/+}$, but not *Anxa2*$^{-/-}$, retinas (Fig. 3a, b). Moreover, cells doubly positive for RPE65 (green) and A2 (red) were present within both the RPE layer and the retinas of dispase-treated *Anxa2*$^{+/+}$ eyes, whereas RPE65 expression was confined to the RPE layer in *Anxa2*$^{-/-}$ dispase-treated eyes (Fig. 3c, d). In addition to vascular SMA-positive cells, *Anxa2*$^{+/+}$ eyes also displayed abundant SMA-positive cells (red), not associated with blood vessels, within the injured retina, and clearly distinct from the associated CD68-positive (green) cells (Fig. 3e, f). In contrast, SMA staining was confined to microvessels, and CD68 staining was nearly absent, in dispase-treated *Anxa2*$^{-/-}$ retinas at two weeks. In *Anxa2*$^{+/+}$, but not *Anxa2*$^{-/-}$ retinas, many RPE65-positive (green) cells appeared to also express SMA (red) (Fig. 3g, h), and SMA-positive cells were found streaming through the retinal wound in *Anxa2*$^{+/+}$ eyes (Fig. 3g, **inset**). Quantitative analysis of immunofluorescent images revealed highly significantly increased cross-reactivity for anti-CD68 ($p = 0.0000$), RPE65 ($p = 0.0041$), and SMA ($p = 0.0000$) in retinas of dispase-treated *Anxa2*$^{+/+}$ versus *Anxa2*$^{-/-}$ mice (Fig. 3i-k). Together, these results indicate that A2-positive, RPE-like cells begin to express SMA and migrate into the retina where macrophage-like cells have already accumulated. In the *Anxa2*$^{-/-}$ eye, on the other hand, macrophages fail to accumulate within the injured retina, and A2-negative RPE cells remain in their original position and are SMA-negative.

Annexin A2 Promotes Macrophage Recruitment in PVR Injury

To further characterize the role of A2 in recruitment of monocyte/macrophages to the site of retinal injury following dispase injection, we rescued lethally-irradiated *Anxa2*$^{+/+}$ and *Anxa2*$^{-/-}$ mice with bone marrow from either *Anxa2*$^{LacZ/+}$ or *Anxa2*$^{LacZ/-}$ knock-in mice (Fig. 4; Suppl. Figure 3). Five weeks later, after verification of engraftment, all four groups of mice underwent intravitreal dispase injection, followed 1 week later by staining of retinal tissue for β-galactosidase, as a reporter for Anxa2 gene activity, and the macrophage marker F4/80. Quantification of the data revealed that, in retinas of either *Anxa2*$^{+/+}$ or *Anxa2*$^{-/-}$ mice that received *Anxa2*$^{LacZ/+}$ bone marrow and were then subjected to PVR, contained significantly higher absolute numbers of F4/80-positive cells compared with those receiving *Anxa2*$^{LacZ/-}$ bone marrow ($p = 0.002$ and $p = 0.039$; Fig. 4a, b, e). In addition, the percentage of X-gal-positive cells that were also positive for F4/80 was significantly increased when the mice were rescued with *Anxa2*$^{LacZ/+}$ versus *Anxa2*$^{LacZ/-}$ bone marrow (66–80% versus 15–38%; $p = 0.009$ and 0.000, respectively, (Suppl. Figure 4). These data demonstrate that A2 expression was required for robust recruitment of macrophages, but not neutrophils, to the injured retina.

To define the potential impact of macrophages recruited into the dispase-injured retina upon RPE cell migration, we seeded *Anxa2*$^{+/+}$ or *Anxa2*$^{-/-}$ primary RPE cells on laminin-coated, 3-micron pore Transwell filters positioned atop wells containing *Anxa2*$^{+/+}$ or *Anxa2*$^{-/-}$ bone marrow-derived macrophages (BMDMs) (Fig. 4f). After 18 hours, we observed significant migration of *Anxa2*$^{+/+}$ RPE cells across the filter, whereas migration of *Anxa2*$^{-/-}$ cells was significantly diminished ($p = 8.9$ E-10). On the other hand, the genotype of BMDMs in the lower chamber did not significantly affect RPE cell migration ($p = 0.1479$). Because we noted that the influx of macrophages was much more robust in *Anxa2*$^{+/+}$ versus *Anxa2*$^{-/-}$ PVR eyes (Fig. 3a, b), we postulated that A2 is required for recruitment of macrophages, but not for their secretion of a factor that might stimulate RPE cell migration. We also noted that induction of migration of human ARPE-19 cells across a laminin barrier by activated human THP-1 cells was significantly inhibited in the presence of tranexamic acid ($p = 0.0005$), an agent that blocks the lysine-binding sites of plasminogen, and thus prevents its interaction with cell surface annexin A2 and its activation to plasmin (Fig. 4g). A control amino acid, glycine, had no effect ($p = 0.9979$). In addition, pre-incubation of ARPE-19 cells with anti-A2 IgG significantly inhibited ARPE-19 cell migration ($p = 0.0057$), whereas non-immune IgG was ineffective. Together, these data indicated that cell surface expression of A2 and generation of plasmin activity on RPE cells is required for macrophage-induced RPE cell migration, whereas macrophage genotype itself did not affect recruitment of RPE cells.

Macrophage-Inflammatory Proteins Drive A2 to the RPE Cell Surface

To further understand how blood-derived macrophages might direct RPE cell migration to sites of retinal injury, we conducted cytokine

https://doi.org/10.1038/s41467-024-52675-x

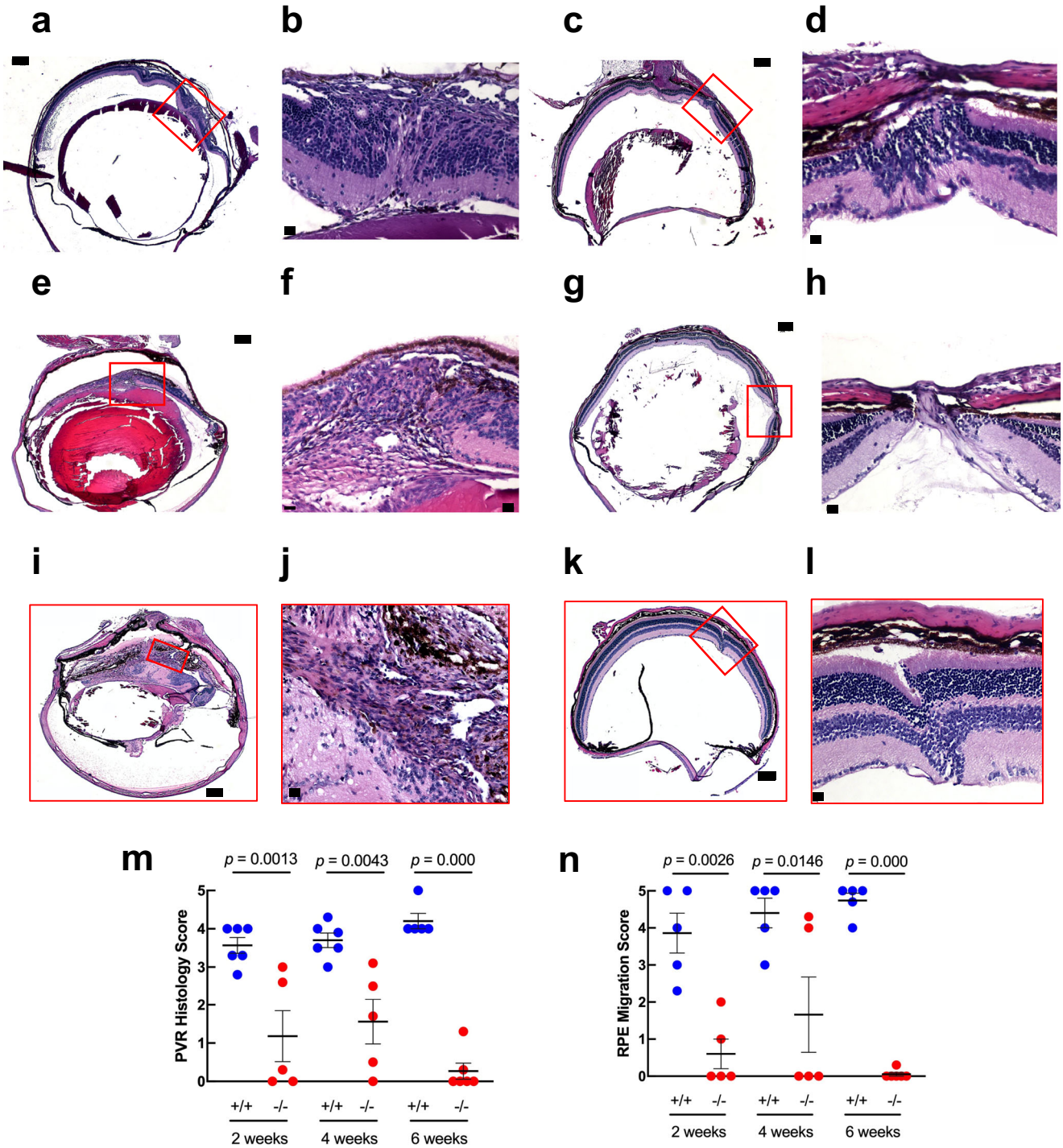

Fig. 1 | Expression of A2 promotes dispase-induced PVR. At two **a**–**d**, four **e**–**h**, or six (**i**–**l**) weeks after intravitreal injection of dispase (0.9 units, OS), *Anxa2*$^{+/+}$ (**a**, **b**, **e**, **f**, **i**, **j**) or *Anxa2*$^{-/-}$ (**c**, **d**, **g**, **h**, **k**, **l**) mice were sacrificed and the eyes harvested, fixed, and embedded. Representative, five-micron, hematoxylin- and eosin- (H and E) stained sections through the injection site (boxed) are shown. Scale bars for **a**, **c**, **e**, **g**, **i**, and **k** are 200 µm, and for **b**, **d**, **f**, **h**, **j**, and **l**, 20 µm. Figures **a**–**d** and **i**–**l** are representative of 3 separate experiments. Figures **e**–**h** are representative of 8 separate experiments. (**m**, **n**) Each point represents the average score for 3 sections from a given mouse; 5 or 6 mice were evaluated in each of the six experimental groups. *Anxa2*$^{+/+}$ and *Anxa2*$^{-/-}$ mice are shown in blue and red, respectively at 2, 4, and 6 weeks. Sections were evaluated by 4 trained observers using a standard algorithm (Suppl. Figure 1) to derive mean ± sem scores for PVR histology (**m**) and RPE migration (**n**). *p* values were determined by one-tailed Student's t test. Source data for **m**, and **n** are provided as a Source Data file.

profiling experiments on pooled retinal homogenates. Screening across a panel of 13 inflammatory cytokines and chemokines revealed 2-3-fold increases in MIP-1α (aka chemokine [C-C motif] ligand 3, CCL3), MCP-1 (monocyte chemotactic protein-1), and TARC (thymus and activation regulated chemokine; aka, CCL17) at 2 days. We focused further analyzes on MIP-1α and MIP-1β, given that elevated levels of both chemokines have been reported in the subretinal fluid and vitreous humor from human subjects with PVR[29–31]. Originally identified in macrophage-like cells as endogenous chemotactic mediators, both MIP-1α and MIP-1β (CCL4) interact with G-protein coupled receptors, CCR1 and CCR5, expressed on a range of cell types to elicit their recruitment to sites of acute and chronic inflammation in disorders

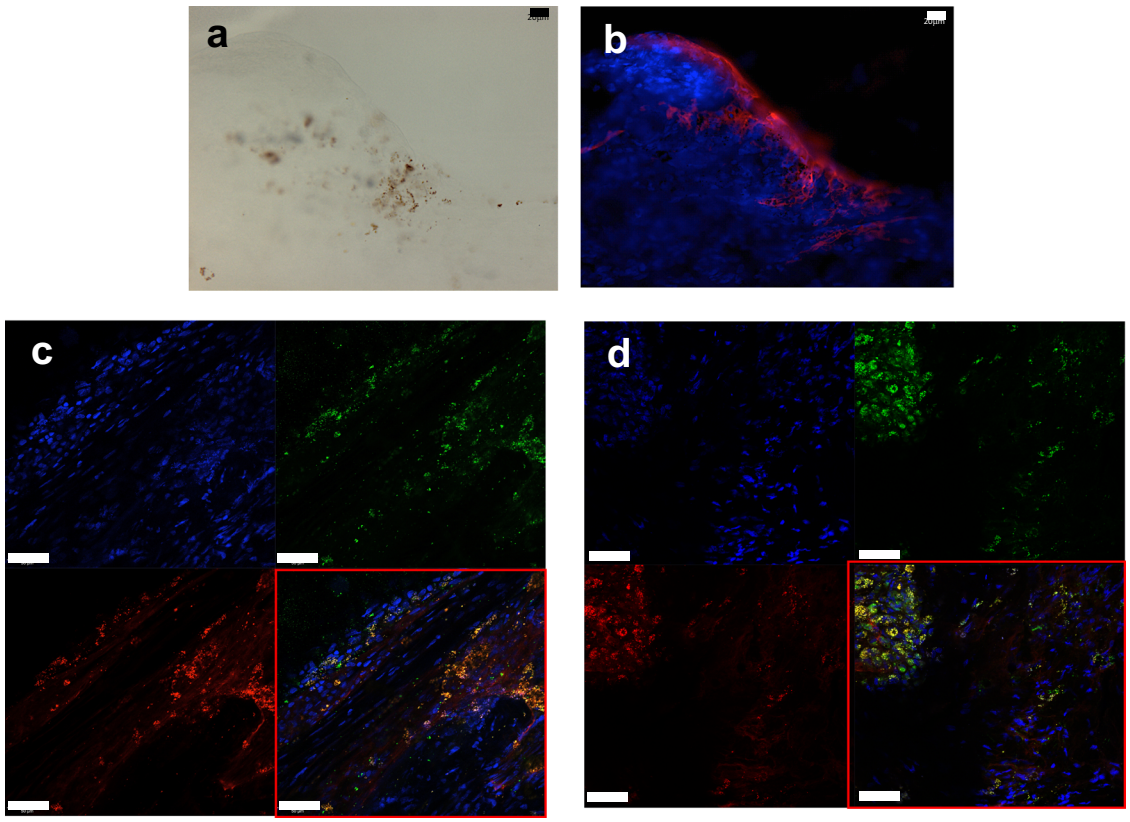

Fig. 2 | Expression of A2 in human epiretinal membranes. Brightfield (**a**) and adjacent immunofluorescence (**b**) images of epiretinal membrane harvested at surgery demonstrate pigment granules, and associated anti-A2 immunoreactive material (**red**) at the vitreal border. DAPI staining (**blue**) reveals the highly cellular nature of the membrane. **c**, **d** Confocal images of sections through a human epiretinal membrane stained with anti-annexin A2 (**red**) and either anti-CD68 (**c**, **green**), or anti-RPE65 (**d**, **green**). Nuclei are stained with DAPI (**blue**). Lower right insets show cellular co-staining for A2 and either CD68 (**c**) or RPE65 (**d**). Figures **a**-**d** are representative of 3 separate samples.

such as asthma, arthritis, multiple sclerosis, and psoriasis, and in wound healing[32–36]. Analyses using specific ELISAs confirmed elevations of both MIP-1α (14-60-fold; $p = 0.0161$) and MIP-1β (2-3-fold; $p = 0.0167$) in *Anxa2*$^{+/+}$, but not *Anxa2*$^{-/-}$, retinas 24 hours after dispase injection (Fig. 4h, i).

In examining the effect of recombinant MIP-1α and MIP-1β on ARPE-19 cell behavior in vitro, we found that each chemokine alone had no significant effect on the rate of migration across laminin-coated filters, whereas the two agents together increased migration approximately 15-fold, suggesting a synergistic effect (Fig. 4j, $p = 2.6$ E-6). In addition, an anti-MIP-1α/β IgG "cocktail" specifically blocked migration of human ARPE-19 cells induced by activated THP-1 macrophages, which produce MIP-1α and MIP-1β (Suppl. Figure 5a,b), by 40–50% (Fig. 4k, $p = 0.0027$). Anti-MIPs also partially blocked *Anxa2*$^{+/+}$ macrophage-induced RPE cell migration (Fig. 4f, $p = 5.2$ E-9). Cultured microglial cells stimulated RPE cell migration, but to less than half the degree observed for THP-1 macrophages (Suppl. Figure 5c). We noted, further, that cultured ARPE-19 cells show strong expression of CCR1, but weak expression of CCR5, the primary receptors for MIP-1α and MIP-1β (Suppl. Figure 6a-c). Resting RPE cells in the mouse retina express low levels of CCR1, which increase significantly 2 weeks after induction of PVR (Suppl. Figure 6d, e); CCR5, on the other hand, was barely detectable in either the uninjured retina or in migrating RPE-65-positive cells after induction of PVR (Suppl. Figure 6f, g). These data suggest that macrophage-derived MIP-1α and MIP-1β may mediate RPE cell migration in the murine retina, most likely via interaction with CCR1, within the first two days of injury.

Next, we explored the mechanism by which MIP-1α and MIP-1β might stimulate RPE cell delamination and migration through the retina and over its vitreal surface in the injured retina (Fig. 5). Previously, we demonstrated that translocation of A2 to the surface of endothelial cells requires Src-mediated tyrosine phosphorylation of A2 at Y24[21]. In the current study, we incubated RPE cells with conditioned medium (CM) from activated THP-1 cells supplemented with or without RPE cell CM. Biotinylation of cell surface proteins, followed by streptavidin capture and immunoblot analysis, revealed that THP-1-derived CM increased RPE cell surface annexin A2 (sA2) 3-4-fold, and that this effect could be significantly inhibited with anti-MIP-1α/β IgG (Fig. 5a, b; $p = 0.0002$). Recombinant human MIP-1α and MIP-1β (rMIPs) strongly stimulated Src activation and tyrosine phosphorylation of A2 ($p = 0.0300$) in a manner that was completely blocked by the Src kinase inhibitor PP2 ($p = 0.0164$), but not the control agent, PP3 (Fig. 5c, d). rMIPs also induced translocation of A2 to the cell surface ($p = 0.0145$) in a Src kinase-dependent manner (Fig. 5e, f). These data indicate that MIP-1α and MIP-1β likely contribute to the development of PVR by enabling Src-dependent translocation of A2 to the RPE cell surface, with subsequent activation of cell surface plasminogen to plasmin, extracellular matrix remodeling, and RPE cell delamination and migration to the vitreal surface.

Blockade of Either A2 or MIP-1 α/β Attenuates Development of PVR

We then pretreated wild type mice with a single anterior chamber injection of anti-A2 versus control IgG 2 days prior to injection of dispase (Fig. 6). Antibodies 1A7 and 2E6 displayed nanomolar affinity for A2 (Suppl. Figure 7), whereas 1D4, produced in the same manner, had no anti-A2 activity and served as a negative control. Both 1A7, and 2E6, but not 1D4, blocked A2-dependent plasmin

https://doi.org/10.1038/s41467-024-52675-x

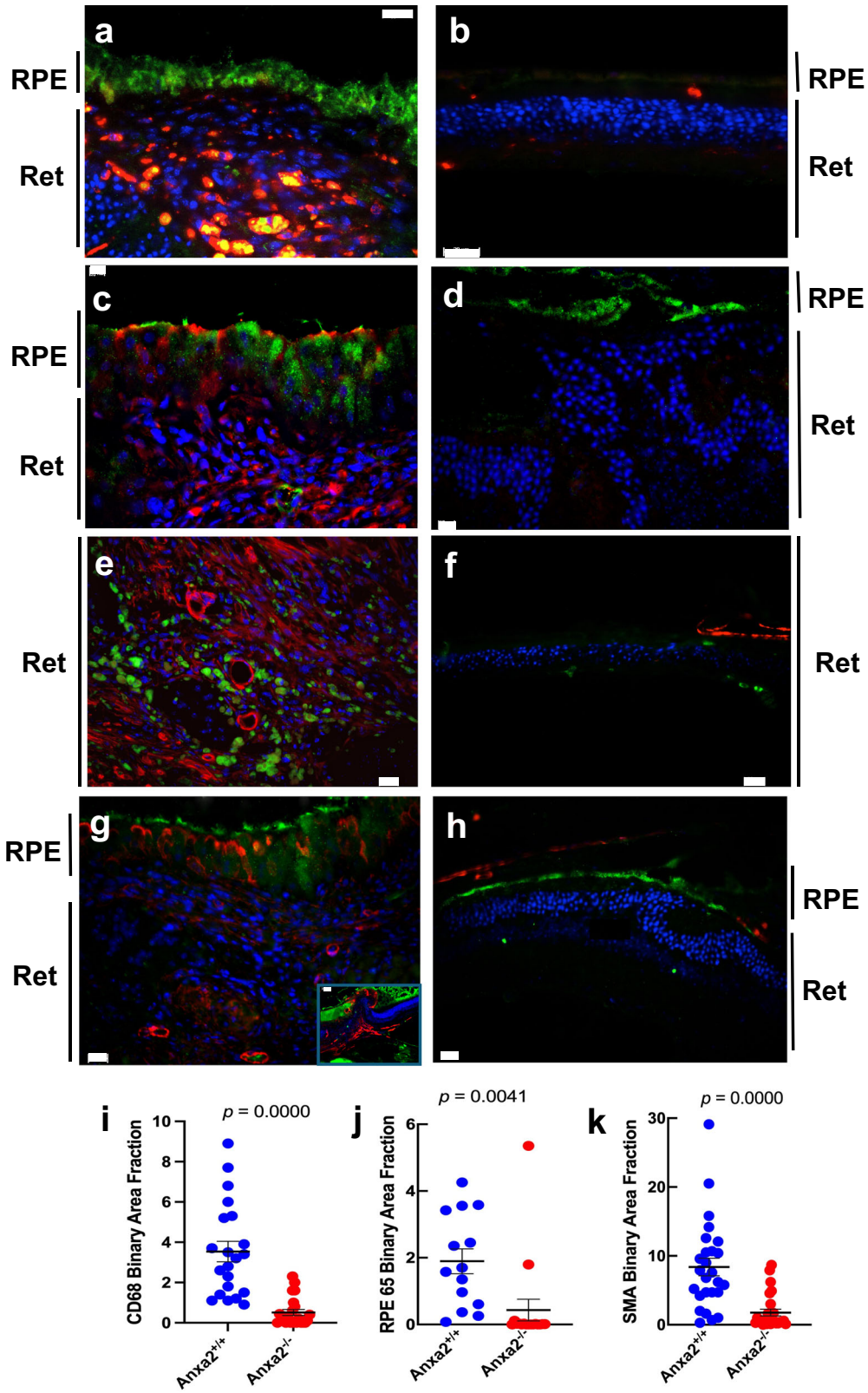

generation in a dose-dependent manner[37]. Analysis of H&E-stained sections of eyes harvested at 2 (Fig. 6a) and 4 (Fig. 6b) weeks revealed that administration of either of two anti-A2 antibodies (1A7, 15 ng, or 2E6, 45 ng) was effective in blocking the development of PVR, whereas neither PBS nor the inactive control (1D4, 45 ng) had any significant effect. Quantitative histologic assessment showed that mice receiving either no antibody or the inactive control (1D4) developed flagrant PVR, whereas overall retinal architecture was preserved and minimal RPE cell migration or epiretinal membrane formation was noted animals receiving anti-A2 IgG as either 2E6 ($p = 0.0273$) or 1A7 ($p = 0.0356$), reflecting extensive retinal disruption, detachment, and contraction, as well as the presence of pigmented RPE cells within the retinal scar and extraretinal tissues ($p = 0.000$ and $p = 0.0001$, respectively, Fig. 6c, d).

Fig. 3 | Immunohistologic evaluation of PVR in *Anxa2*$^{+/+}$ and *Anxa2*$^{-/-}$ mice. Eyes from *Anxa2*$^{+/+}$ and *Anxa2*$^{-/-}$ mice were harvested 2 weeks after dispase injection, and representative sections (5-µm) deparaffinized and stained with antibodies directed against CD68, A2, or RPE65 in different combinations. Nuclei are stained with DAPI (**blue**). **a**, **b** CD68 (**red**, rabbit anti-CD68, Abcam AB125212; 1:200)with donkey anti-rabbit Cy3, Jackson ImmunoResearch Laboratories, 711-165-152; 1:300) and A2 (**green**, goat anti-annexin A2, R&D Systems AF3928; 1:50 with donkey anti-goat Alexa 647, Invitrogen A21447; 1:100) staining in *Anxa2*$^{+/+}$ (**a**) and *Anxa2*$^{-/-}$ (**b**) retinas. Cells co-expressing CD68 and A2 are abundant in *Anxa2*$^{+/+}$ retinas, but rare in *Anxa2*$^{-/-}$ retinas. **c**, **d** A2 (**red**, rabbit anti-annexin A2, Cell Signaling 8235S; 1:300 with donkey anti-rabbit Cy3, Jackson ImmunoResearch Laboratories 711-165-152; 1:300) and RPE-65 (**green**, mouse anti-RPE-65, Novus NB100-355; 1:150 with donkey anti-mouse Alexa 647, Invitrogen A31571; 1:100) staining in *Anxa2*$^{+/+}$ (**c**) and *Anxa2*$^{-/-}$ (**d**) retinas. A2 is expressed in RPE-65-positive cells posterior to the retina and within the retina of the dispase-injected *Anxa2*$^{+/+}$ eye, whereas RPE-65 expression is confined to the posterior retina in the absence of A2 in the dispase-injected *Anxa2*$^{-/-}$ eye. **e**, **f** Staining for smooth muscle actin (**red**, mouse anti-SMA, Cy3, Sigma C6198; 1:50) and CD68 (**green**, rabbit anti-CD68, Abcam AB125212; 1:200 with donkey anti-rabbit Cy5, Jackson ImmunoResearch Laboratories; 711-175-152; 1:100) shows that they are not expressed in the same cells in retinas from either *Anxa2*$^{+/+}$ (**e**) or *Anxa2*$^{-/-}$ (**f**) dispase-injected mice. SMA labels blood vessel smooth muscle cells, fibroblasts, and fibroblast-like cells in the damaged retina, whereas CD68, expression in presumptive macrophages and microglial cells, remains separate. In the *Anxa2*$^{-/-}$ eye, SMA is expressed in blood vessels; CD68-positive cells are rare. **g**, **h** Staining for SMA (**red**, rabbit anti-SMA, Cell Signaling 19245 T; 1:300 with donkey anti-rabbit Cy3, Jackson ImmunoResearch Laboratories 711-165-152; 1:300) and RPE-65 (**green**, mouse anti-RPE-65, Novus NB100-355; 1:150 with donkey anti-mouse Alexa 647, Invitrogen A31571; 1:100) in *Anxa2*$^{+/+}$ (**g**) and *Anxa2*$^{-/-}$ (**h**) dispase-injected eyes. In the *Anxa2*$^{+/+}$ retina, cells doubly positive for RPE and SMA are found in the RPE layer and also within the retina. In *Anxa2*$^{-/-}$ dispase-injected eyes, RPE cells lack SMA expression and do not enter the retina. The inset in **g** shows SMA-positive cells (**red**) migrating through the injection site of a dispase-injected *Anxa2*$^{+/+}$ eye. Scale bars are 20 µm for **a**-**h** and 50 µm for inset in (**g**). **i**, **j**, **k** Quantification of fluorophore signals based on binary area fraction for CD68, RPE65, and SMA signals, respectively, in *Anxa2*$^{+/+}$ (blue) and *Anxa2*$^{-/-}$ (red) retinal tissue across 14-27. The data in (**i**) represent analysis of 21 fields from 5 *Anxa2*$^{-/-}$ mice, and 23 fields from 5 *Anxa2*$^{+/+}$ mice. The data in (**j**) represent analysis of 14 fields from 5 *Anxa2*$^{-/-}$ mice, and 17 fields from 5 *Anxa2*$^{+/+}$ mice. The data in (**k**) represent analysis of 26 fields from 5 *Anxa2*$^{-/-}$ mice, and 27 fields from 5 *Anxa2*$^{+/+}$ mice. Shown for (**i**, **j**, **k**) are mean values ± SE, with *p* values determined by one-tailed Student's t test. Source data for (**i, j**, and **k**) are provided as a Source Data file.

These data indicate that blockade of A2 may be a useful approach to the prevention of PVR in the setting of retinal injury.

Finally, we tested the ability of antibodies directed against MIP-1α and MIP-1β to prevent dispase-induced PVR (Fig. 7a, b). Wild type mice received anti-MIP-1α, anti-MIP-1β, or a combination of the two in the anterior chamber 1 day after intravitreal injection of dispase, and eyes were harvested at 4 weeks. Both PVR histology and RPE migration scores were highly significantly reduced upon pretreatment with anti-MIPs ($p = 0.002–0.030$; Fig. 7a, b).

Discussion

The data presented here demonstrate for the first time that annexin A2 plays an essential role in the development of PVR in a standard mouse model. *Anxa2*$^{-/-}$ mice are highly resistant to dispase-induced PVR (Fig. 1), showing markedly reduced recruitment of macrophage-like cells to the injured retina, and failure of RPE cells to delaminate and migrate through the retina (Figs. 3 and 4). In vitro, both human and murine macrophage-like cells can direct migration of A2-expressing RPE cells, but not A2-negative RPE cells (Fig. 4f, g). Macrophage-secreted MIP-1α and MIP-1β appear to induce migration of RPE cells in vitro by activating Src, and inducing tyrosine phosphorylation and translocation of A2 to the RPE cell surface (Fig. 5). A2-related plasmin activity, possibly with downstream activation of matrix metalloproteases, appears to facilitate RPE cell delamination and migration in an EMT-like process (Fig. 4g). Interestingly, A2-mediated plasmin generation appears to be necessary for this migration, as it was for the EMT-like process that underlies avian cardiac development[25]. The finding that A2-expressing RPE and macrophage-like cells are present within human PVR membranes removed at surgery (Fig. 2) suggests that A2 may play a central role in human PVR as well.

There is abundant evidence that cell surface plasmin activity enables recruitment of macrophages to sites of inflammation. Thioglycollate-induced macrophage recruitment to the peritoneal cavity requires plasmin-mediated fibrinolysis[38,39]. Macrophage recruitment may be supported by a constellation of at least 4 different cell surface plasminogen receptors, including α-enolase, histone H2B, Plg-R_{KT}, and annexin A2/S100A10 tetramer[40,41], which mediates plasminogen dependent matrix remodeling by human monocytes and macrophages[18,42]. The innermost layer of Bruch's membrane, a pentalaminar structure that supports adhesion of RPE cells[43], is composed of collagen IV, heparan sulfate proteoglycans, laminin, and fibronectin[43,44], the latter two of which are known plasmin substrates[45]. Thus, it is possible that development of active plasmin at the RPE cell surface could facilitate its detachment and migration toward a chemotactic stimulus in an EMT-like process.

Taken together, our data suggest that macrophages recruited into the injured retina initiate delamination and directed migration of RPE cells through the elaboration of MIP-1α and MIP-1β (Fig. 7c-h). In the *Anxa2*$^{+/+}$ mouse, injury-associated macrophages elaborate these mediators (Fig. 7d, e), which, likely through interaction the CCLR1 pathway, activate Src kinase, which, in turn, stimulates phosphorylation of annexin A2; phospho-A2 may then translocate to the cell surface where it supports localized plasmin activity (Fig. 7f). In an EMT-like process, cell surface plasmin then likely allows RPE cells to undergo a transition to migratory smooth muscle-like cells (Fig. 7g). Transformed, SMA-positive RPE cells then secrete scar-producing matrix proteins, resulting in the fibrotic response characteristic of PVR (Fig. 7h). It is conceivable that A2 may mediate other fibrotic responses, such as renal or pulmonary fibrosis, hepatic cirrhosis, and systemic sclerosis. Ultimately, A2 may represent a tractable target for the prevention of these processes.

Methods

In compliance with relevant ethical regulations, all animal work was approved by the Weill Cornell Medicine Institutional Animal Care and Use Committee (IACUC), and all studies on human tissue were performed in accordance with a protocol approved by the Weill Cornell Medicine Institutional Review Board.

Dispase model

Male and female *Anxa2*$^{+/+}$ and *Anxa2*$^{-/-}$ C57Bl/6 mice, aged 2–4 months[28] were housed in the Weill Cornell Medicine Research Animal Resource Center, under standard conditions including a 12-hr light-dark cycle (lights on at 6 AM and off at 6 PM), ambient temperature of 18–23 °C, and humidity of 40–60%. Mice were provided with irradiated rodent PicoLab Lab Diet 20 (#5053) on an *ad libitum* basis. Following general anesthesia with isoflurane, one drop each of 0.5% proparacaine HCl, for local anesthesia, as well as 2.5% phenylephrine and 1% tropicamide, for iris dilatation, were applied topically to the left eye in accordance with an IACUC-approved protocol. A single intravitreal (IVT) injection of either sterile phosphate buffered saline (PBS) or dispase (Worthington Biochemicals; final concentration 0.1-0.3 U/µl PBS; 3 µl) was made under microscopic control with a Hamilton syringe, fitted with a 30 G1/6 needle in the dorsal nasal quadrant of the left eye, at the level of the equator[26]. Only the beveled tip was allowed to enter the vitreal cavity. At specific time points over the ensuing 2-6 weeks, mice were

https://doi.org/10.1038/s41467-024-52675-x

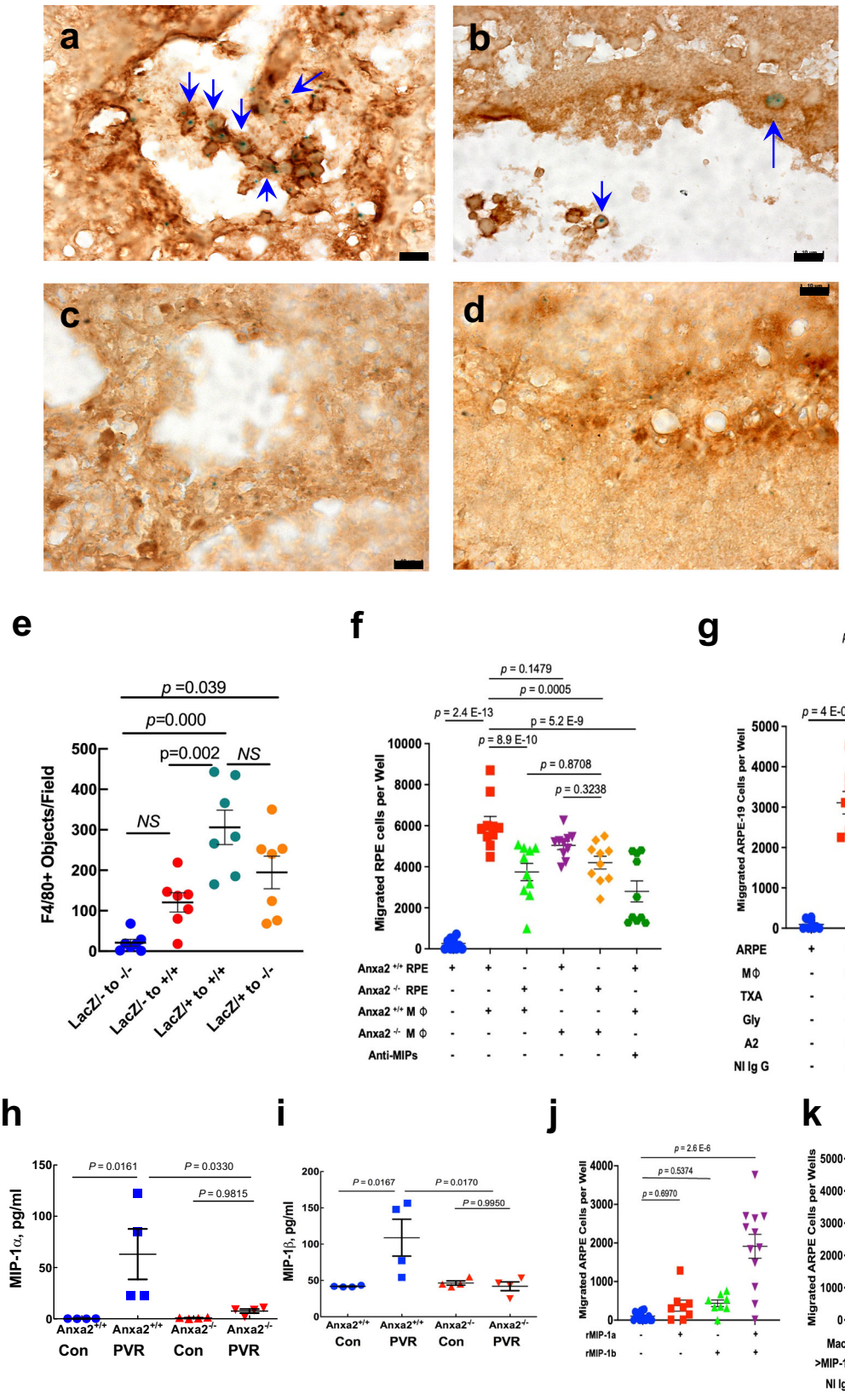

euthanized by CO_2 inhalation, and the eyes harvested. Pre-incubation of dispase with A2 had no effect on its ability to proteolyze purified laminin, a major component of Bruch's membrane[44]. For antibody injection, *Anxa2*$^{+/+}$ mice received 3 µl of anti-annexin A2 antibody 1A7 (5 µg/ml), 2E6 (15 µg/ml), or 1D4 (15 µg/ml) into the anterior chamber of the left eye 2 days before injection of IVT dispase.

Experimental animals

Strain C57Bl/6 *Anxa2*$^{-/-}$ mice were developed in the Hajjar Lab[28]. For the experiments reported, 42% of mice were female and 58% male, and no sex differences in experimental outcomes were noted. Offspring of homozygous matings were genotyped by PCR of tail tip DNA using nucleotides A2WT (5′-GCA, CAG, CAA, TTC, ATC, ACA, CTA, ATG,TCT,

Fig. 4 | Role of A2 expression in macrophage-mediated PVR. *Anxa2*$^{+/+}$ (**a**, **c**) and *Anxa2*$^{-/-}$ (**b**, **d**) mice underwent bone marrow ablation and rescue with either *Anxa2*$^{LacZ/+}$ (**a, b**) or *Anxa2*$^{LacZ/-}$ (**c, d**) bone marrow. At five weeks, mice received intravitreal dispase. Eyes were harvested 1 week later and sections stained for expression of X-gal (**blue**) and F4/80 (**dark brown**). Arrows (**a, b**) indicate doubly-positive cells. Scale bars are 10 μm for **a**–**d**. Images in **a**-**d** are representative of 3 separate experiments. **e** Frozen, OCT-embedded sections (40x) of retinas from mice transplanted with bone marrow that express lacZ were detected by X-Gal staining and the macrophage marker, rabbit anti-F4/80 (Abcam AB111101; 1:100 with ImmPRESS® HRP Goat Anti-Rabbit IgG Polymer Detection Kit, Peroxidase, Vector Laboratories, MP-7451; Ready-to-Use Kit) and examined independently by 3 masked observers. The enumerated F4/80-positive objects per 40x field were plotted for 7 sections representing 2–4 mice per group. **f** Murine primary RPE cells (passage 5; 2×10^4 cells/well; *Anxa2*$^{+/+}$ or *Anxa2*$^{-/-}$) were cultured on 3 μm, laminin-coated Transwell filters positioned above chambers containing *Anxa2*$^{+/+}$ or *Anxa2*$^{-/-}$ bone marrow-derived macrophages (2×10^5 cells/well). At 18 h, residual RPE cells from the upper surface of the filter were removed, and migrated cells estimated as described (Methods). For antibody blocking, polyclonal goat anti-mMIP-1α (1 μg/ml) and monoclonal rat anti-mMIP-1β (1 μg/ml) were added to the lower chamber. Shown are data, combined from 2 separate experiments, for 10 wells/group. (**g**) THP-1-induced migration of ARPE-19 cells plated atop laminin-coated filters was assessed at 18 h in the presence of mouse anti-human A2 IgG (1 μg/ml), mouse IgG1 control (NI IgG, 1 μg/ml), tranexamic acid (TXA, 2 mM), or glycine (2 mM), as described in **f**. Shown are data, combined from 2 separate experiments, for 7–11 wells/group. **h**, **i** Extracts of retinas (4 retinas/group) from non-injected control mice or those receiving intravitreal dispase were assayed at 24 h for MIP-1α (**h**) and MIP-1β (**i**) by ELISA. **j** ARPE-19 cells atop laminin-coated Transwell filters were stimulated with 250 ng/ml rhMIP-1α and/or 250 ng/ml rhMIP-1β in the lower chamber. Cell migration was quantified as in **f**. Shown are data, combined from 4 separate experiments, for 8–16 wells/group. **k** THP-1-induction of ARPE-19 cell migration was evaluated as in **f** in the presence of goat anti-human MIP-1α/β (1 ug/ml) versus non-immune goat IgG. Shown are data, combined from 4 separate experiments, for 7-16 wells/group. Shown for (**e**-**k**) are mean values ± SE, with *p* values determined by unpaired one-way ANOVA and the post hoc Tukey test. Source data for **e**-**k** are provided as a Source File.

TCT, TG-3′), A2KO (5′-GCT, GAC,TCT, AGA,GGA,TCC,CC-3′), and Anint2 (5′-TGC, GCC, ACC, ACG, CCC, GGC, TTG, TGC, TTG, CCA, C-3′), resulting in 221- and 304-bp bands for *Anxa2*$^{-/-}$ and *Anxa2*$^{+/+}$ genotypes, respectively.

For generation of *Anxa2*$^{LacZ/+}$ and *Anxa2*$^{LacZ/-}$ mice, the pSP72 (Promega, #P2191) targeting vector was modified to contain a *Not I* restriction site for linearization (Suppl. Figure 3). The positive neomycin resistance selector, PGKneobpA (NeoR) and negative PGKdtabpA gene (diphtheria toxin A, DTA) selector were subcloned from the PGKneoF2L2DTA vector (Addgene, #13445) and incorporated into the targeting vector. A 3.44-kb *Sac I - Sal I* genomic fragment containing the murine *Anxa2* promoter and portions of intron 2 and exon 3 up to the ATG site was introduced into *Sac I - Sal I* sites upstream of the LacZ expression cassette (*SDK-lacZ-pA)* and the *frt* floxed PGKneobpA cassette in the modified pSP72 vector, resulting in an *Anxa2* promoter-driven *LacZ* gene replacing the *Anxa2* coding region. The *Anxa2* genomic fragments were subcloned from the Invitrogen BAC clone 85I8 template. A second 3.4-kb *Sal I - Xho I Anxa2* fragment including part of *Anxa2* intron 4 was subcloned into the *Sal I* site downstream of the NeoR gene, but upstream of the DTA gene. Finally, the 3.44-kb *Anxa2* left arm and 3.4-kb *Anxa2* right arm flanking the LacZ and the NeoR gene were created to replace the original *Anxa2* sequences, while the *DTA* gene remained outside the regions of *Anxa2* homology.

The targeting vector, pSP-AnxA2::LacZ, was linearized with *Not I* and electroporated into CY2.4 embryonic stem (ES) cells derived from albino B6 mice at the Rockefeller Gene Targeting Resource Center. ES clones were selected by G418 (neomycin, 200 μg/ml, GIBCO/BRL) resistance and screened by Southern blot hybridization. *Sac I*-digested or *Pvu II*-digested ES DNA was electrophoresed on 0.8% agarose gels, and blotted onto nylon membranes. A 378-bp PCR product of LM63 (5′-TTT,GCA,GAG,GCC,TCT,CGC,TTG-3′) and LM64 (5′-AAC,AGC,TG-C,AAC,AAC,GGA,ACC-3′) primers representing sequences downstream of the targeting vector sequence, detected 9.8-kb and 8-kb fragments of wild-type and mutant alleles, respectively, and was used to probe *Sac I*-digested DNA. Another 363-bp PCR product of LM56 (5′-ACA,-CAC,AGG,CCG,GAA,GCT,CAG-3′) and LM57 (5′-TGC,AGT,GCC,AGT,-GAA,GTC,TCT,GG-3′), representing sequences upstream of the targeting vector sequence and detecting 5.4-kb and 4.4-kb fragments of wild-type and mutant alleles, respectively, was employed as the left probe for *Pvu II*-digested DNA.

Eight out of 200 clones were identified as positive by Southern blot hybridization. Of these, two that contained the disrupted allele were introduced into blastocysts of C57Bl/6 embryos and injected into the uteri of pseudopregnant dams. Chimeric males were identified based on agouti coat color, and then mated with C57Bl/6 females. Agouti offspring were genotyped by Southern hybridization as described above. A 363-bp fragment, representing sequences external to the targeting vector sequence and detecting 5.4-kb and 4.4-kb fragments of wild-type and mutant alleles, respectively, was used as the left probe for *Pvu II*-digested DNA. A 378-bp fragment, representing sequences external to the targeting vector sequence and detecting 9.8-kb and 8-kb fragments of wild-type and mutant alleles, respectively, was employed as the right probe for *Sac I*-digested DNA.

For PCR genotyping of DNA isolated from tail biopsies, oligonucleotide primers included LM29 (5′-TGG,TCT,GTG,GAC,ACC,TAT,TTA,CTT, AG-3′) located in intron 3 and thus specific for wild-type, LM32 (5′-CAG,AGT,TCA,TCT,GTG,CAG,TC-3′) located in the A2 right arm and therefore common to both genotypes, and LM79 (5′-GTC,AGG,TCC,ACG,ACC,CAA,GCT-3′) located in PGKneobpA cassette and specific for the targeted allele. LM79 and LM32 generate a 325-bp mutant band, while LM29 and LM32 generate a 595-bp wild type band.

Anxa2$^{lacZ/+}$ heterozygotes were interbred to obtain *Anxa2*$^{lacZ/+}$ and *Anxa2*$^{lacZ/lacZ}$ knock-in mice. Through western blot analysis, *Anxa2*$^{lacZ/lacZ}$ knock-in mice were confirmed to lack A2 protein expression. To remove the PGKneo cassette, *Anxa2*$^{lacZ/+}$ heterozygous mice were crossbred with Flpe mice (Jackson Laboratories, #003946). PGKneo-free *Anxa2*$^{lacZ/+}$ heterozygotes were maintained as PGKneo-free *Anxa2*$^{lacZ/+}$ reporter mice, and were used in the present study. LacZ forward (5′- ATA,CGC,CGA,ACG,ATC,GCC,AGT,TCT-3′) and LacZ reverse (5′-CAC,TAC,GCG,TAC,TGT,GAG,CCA,GAG-3′) primers were used for genotyping PGKneo-free *Anxa2*$^{lacZ/+}$ mice. To generate *Anxa2*$^{lacZ/-}$ mice, PGKneo-free *Anxa2*$^{lacZ/lacZ}$ mice were bred with *Anxa2*$^{-/-}$ mice, and genotypes verified.

Histologic evaluation

Eyes were enucleated, and the nasal-most aspect of the cornea marked with a cautery dot within a plane that also included the injection site and the optic nerve head. The eyes were fixed overnight in 4% paraformaldehyde (PFA) for cryosections, and in Davidson fixative for paraffin sections. For cryosectioning, fixed tissue was placed in 30% sucrose in PBS prior to infiltrating with optimal cutting temperature (OCT)/30%sucrose (2/1:v/v) and freezing in liquid N_2-cooled isopentane. For paraffin sectioning, fixed eyes were place in 70% ethanol for paraffin embedding and sectioning. Five- to seven-micron thick serial sections were cut in a sagittal plane, and mounted on numbered glass slides until the injection site (IS) was identified and verified by microscopic inspection. The most central IS-containing slide was stained with hematoxylin and eosin (H & E). Each slide contained 6-12 sections.

For histologic scoring of H & E-stained tissue, ten sections from within 5 microns of the injection site were evaluated in a double-blind manner by 2–4 trained, masked observers, and scored according to a

https://doi.org/10.1038/s41467-024-52675-x

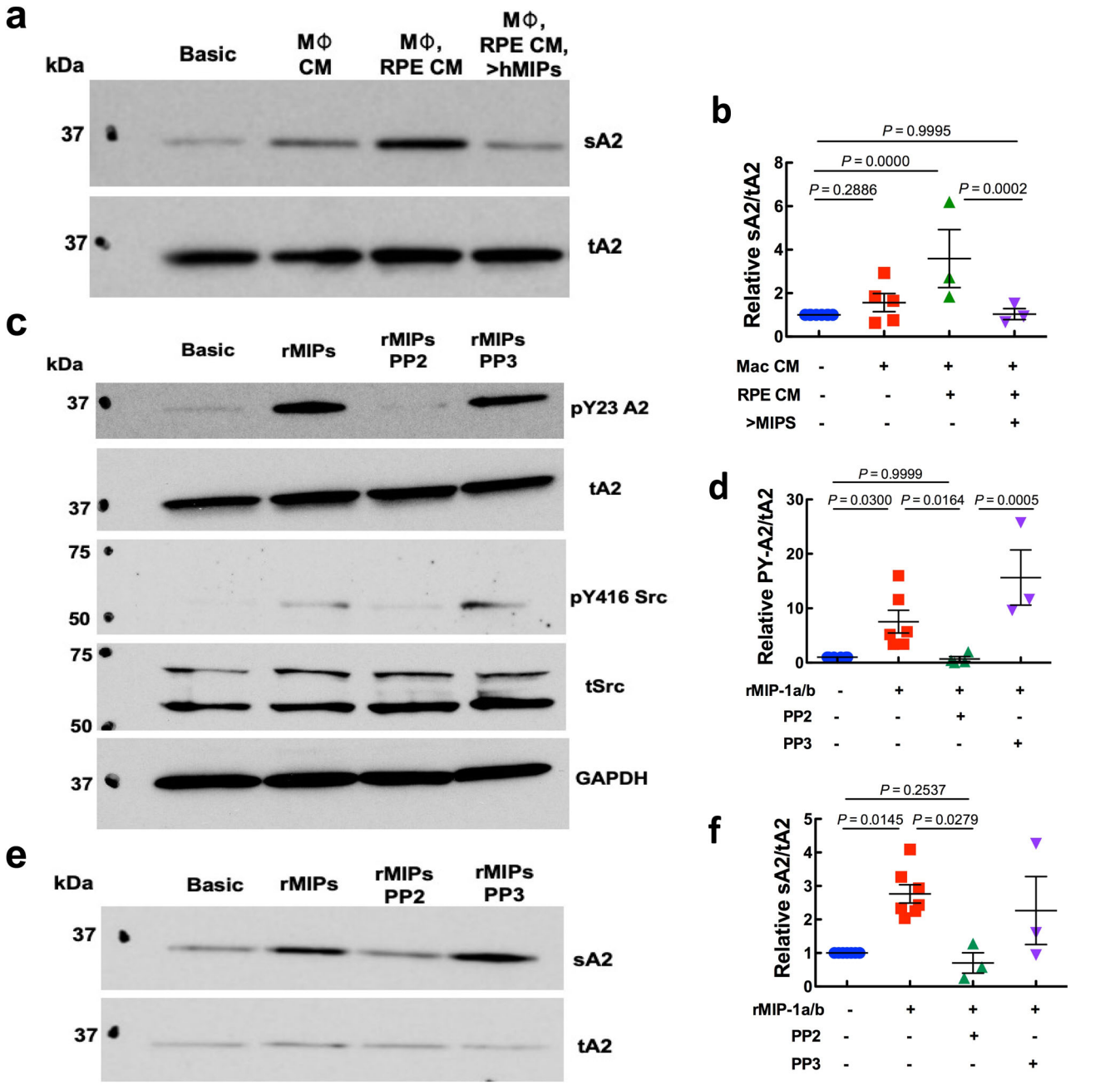

Fig. 5 | MIPs induce Src-dependent tyrosine phosphorylation and translocation of A2 to the cell surface. a ARPE-19 cells were incubated for 18 h with basic medium (**Basic**), activated THP-1 cell conditioned medium (CM), or THP-1 CM with RPE CM with or without addition of anti-human MIP-1α/β or non-immune IgG. Cell surface A2 (sA2) was labeled using membrane impermeable biotinylation and captured with NeutrAvidin agarose beads. Labeled cell surface proteins were resolved by SDS-PAGE and cell surface (sA2) and total cell lysate A2 (tA2) probed by immunoblot with mouse (BD #610069) or rabbit (Cell Signaling #8235) anti-A2 IgG. **b** Pixel density of immunoblotted bands from 3-5 separate experiments were quantified and normalized to the unstimulated sample (**Basic**). **c** ARPE-19 cells were incubated with basic media with or without recombinant human MIP-1α/β (MIPs, 200 ng/ml each), and with or without the Src kinase inhibitor PP2 or its control PP3 (10 μM, 3 h). Cell lysates were probed for pY23-A2, tA2, pY416 activated Src, total Src (tSrc), and GAPDH, as a loading control. **d** Pixel density of immunoblotted bands from 3-6 separate experiments were quantified and normalized to the unstimulated sample (**Basic**). **e** ARPE-19 cells were incubated with or without recombinant human MIP-1α/β (MIPs, 200 ng/ml each) in the presence or absence of PP2 or PP3, as in (**c**). **f** Pixel density of immunoblotted bands from 3–7 separate experiments were quantified and normalized to the unstimulated sample (**Basic**). Shown for (**b, d, f**) are mean values ± SE, with *p* values determined by unpaired one-way ANOVA and the post hoc Tukey test. Source data for (**b, d**, and **f**) are provided as a Source File.

standard rubric that quantified the degree of retinal detachment, disorganization of retinal cell layers, and epiretinal membrane formation (Suppl. Figure 1a). RPE cell migration was evaluated in a separate scoring system based on the presence or absence of RPE cells within the retina, over the vitreal surface of the retina, or within the extraretinal tissues (Suppl. Figure 1b). Across all analyses, interobserver variability averaged 10.4 ± 3.1%.

For β-galactosidase staining of tissue following bone marrow-transplantation, mice were deeply anesthetized with isoflurane and Avertin, and extensively perfused with PBS containing 0.10 g/L CaCl2 and 0.10 g/L MgCl2•6H2O (PBS-CM). The eyes were enucleated and fixed for 30 minutes in 2% PFA in 0.1 M phosphate buffer (PB, pH 7.2). The cornea and lens were removed, and the eyes fixed for an additional 1.5 h in 2% PFA/0.1 M PB at room temperature (RT). After fixation, eyes

https://doi.org/10.1038/s41467-024-52675-x

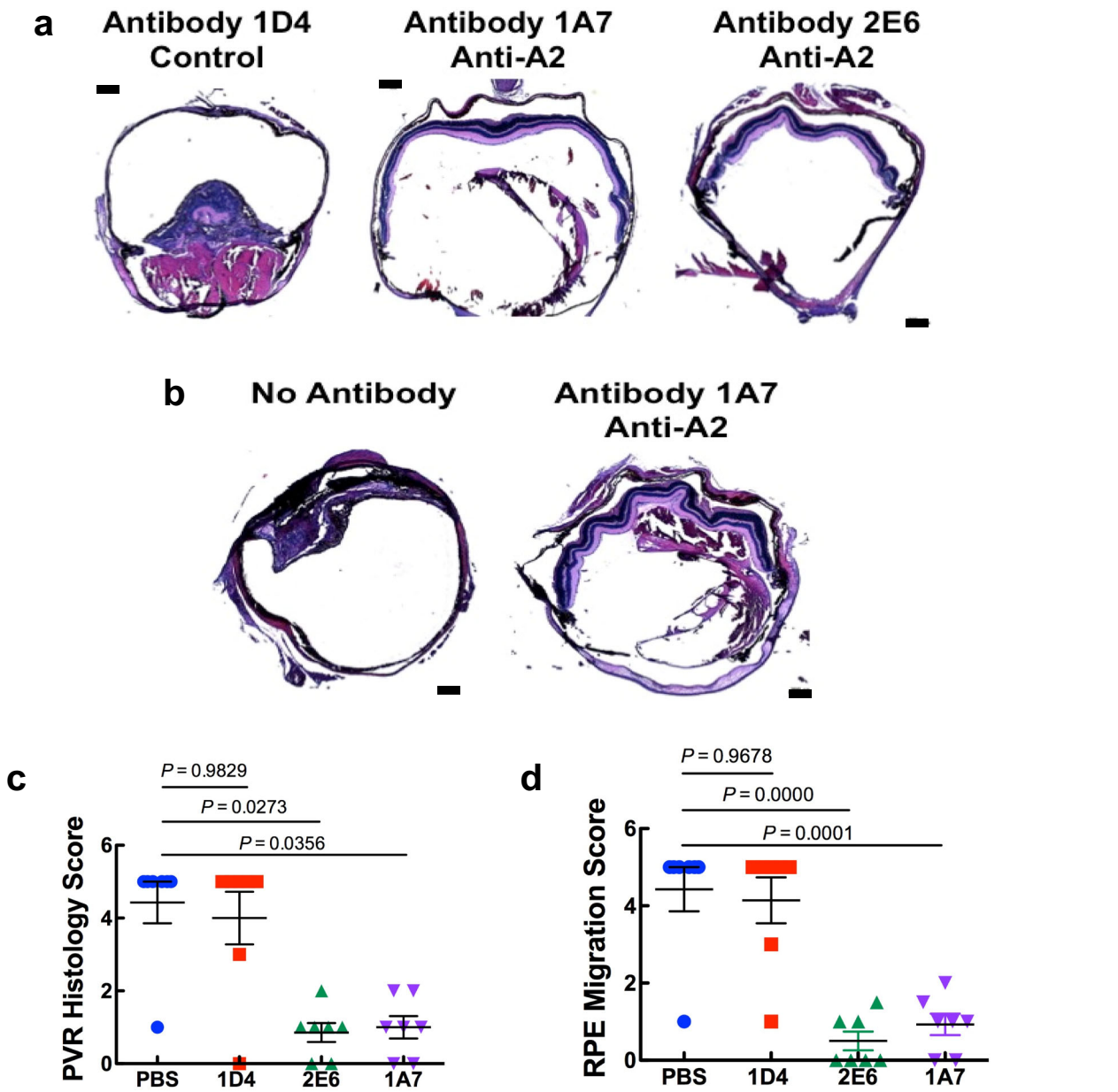

Fig. 6 | Effect of anti-annexin A2 IgG pretreatment on dispase-induced PVR. **a**, **b** Wild type C57Bl/6 mice were pretreated with an anterior chamber injection of anti-A2 IgG (1A7 or 2E6), control IgG (1D4), or PBS, two days prior to intravitreal dispase injection. At 2 (**a**) and 4 (**b**) weeks, the eyes were harvested, fixed, embedded, sectioned, and stained with H and E. Scale bars for (**a** and **b**) are 200 um. PVR histology (**c**) and RPE migration (**d**) scores were recorded by trained, masked observers. Shown for (**c** and **d**) are mean ± SE, $n = 7$ animals/group. p values were determined by unpaired one-way ANOVA and the post hoc Tukey test. Source data for (**c** and **d**), are provided as a Source File.

were washed three times in PB, transferred to 30% sucrose in PB (18 h), placed in OCT/30% sucrose (2:1 v:v) for 30 min, embedded in fresh OCT/30% sucrose. Eight-micron, sagittal cryostat sections were stored in −20 °C.

Prior to staining, sections were thawed, fixed with 0.2% glutaraldehyde, 0.5 mM EGTA, 100 mM $MgCl_2$ in PBS (10 min, RT), washed three times with LacZ wash buffer (PBS, pH 7.3, 2 mM $MgCl_2$, 0.01% sodium deoxycholate, 0.02% Nonidet P-40), incubated with X-gal solution (5 mM potassium ferricyanide, 5 mM potassium ferrocyanide, and 0.1 mg/ml 5-bromo-4-chloro-3-indolyl-b −galactopyranoside from a 25 mg/ml stock solution in formamide) in LacZ wash buffer (37 °C, 18 h, protected from light). The sections were next rinsed three times with PBS, blocked with 2% H_2O_2 (30 min), rinsed three times with PBS, blocked with 2.5% normal goat serum (goat anti-rabbit ImmPRESS HRP kit, Vector Laboratories, MP-7451; 20 min, RT), and incubated with rabbit anti-F4/80 (1:100, Abcam AB111101 in 1% BSA/PBS, 18 h, 4 °C). The sections were then rinsed with PBS, incubated with goat anti-rabbit secondary IgG (goat anti-rabbit ImmPRESS HRP kit, Vector Laboratories, MP-7451; 30 min, RT), rinsed again, treated with ImmPACT DAB (Vector Laboratories, SK-4105; 1-2 min), rinsed in water, air dried, and coverslipped using Vecta Mount (Vector Laboratories, H-5000-60).

For immunohistologic staining, paraffin sections were deparaffinized, subjected to high heat antigen retrieval (100 mM Tris HCl, pH 9, 1 mM EDTA) and RPE pigment bleaching (125 µl formamide, 2 ml dH2O, 125 µl 20X SSC buffer, 409 µl 30% H_2O_2; 20 min at 2.5 inches from direct light), and then treated with cold methanol (-20 °C, 10 min). After rinsing (PBS-CM), sections were blocked (5% donkey serum, 1% BSA, 0.1% Triton X-100 in PBS-CM), and primary antibodies applied overnight (4 °C, 5% donkey serum, 1% BSA, 0.05% Tween-20 in

https://doi.org/10.1038/s41467-024-52675-x

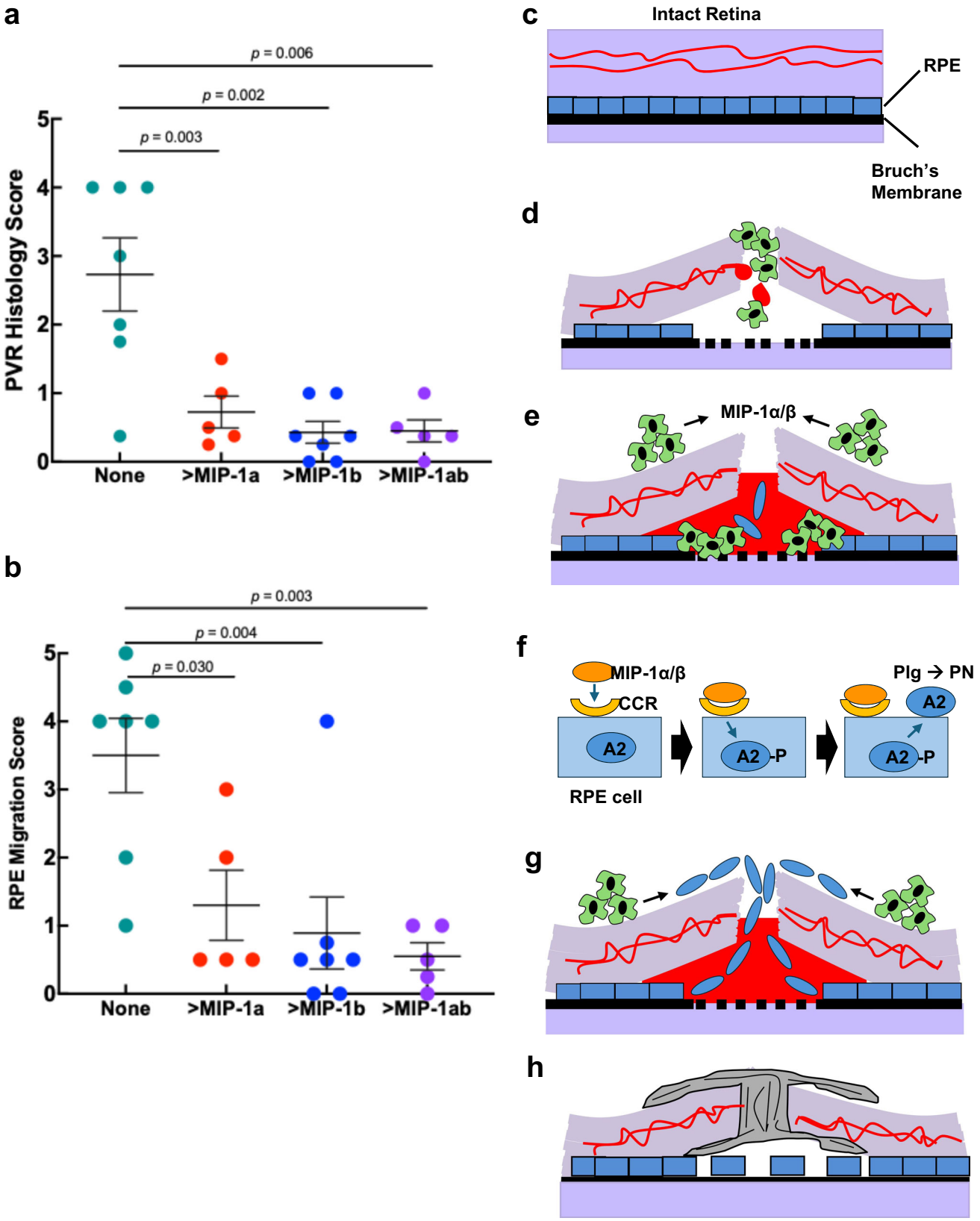

PBS-CM), with the exception of mouse anti-SMA Cy3 (21 °C, 5 min). Primary antibody combinations included mouse anti-RPE-65 (Novus NB100-355; 1:150) with rabbit anti-annexin A2 (Cell Signaling 8235S; 1:300), rabbit anti-CD68 (Abcam AB125212; 1:200) with goat anti-annexin A2 (R&D Systems AF3928; 1:50), mouse anti-RPE-65 (Novus NB100-355; 1:150) with rabbit anti-SMA (Cell Signaling 19245 T; 1:300), and mouse anti-SMA (Cy3 Sigma C6198; 1:50) with rabbit anti-CD68 (Abcam AB125212; 1:200). After washing again, sections were treated with secondary antibodies (37 °C, 30 min; 5% donkey serum, 1% BSA, 0.05% Tween-20 in PBS/CM) followed by DAPI (1:10,000, 5 min). Secondary antibodies included donkey anti-mouse Alexa 647 (Invitrogen; A31571, 1:100), donkey anti-rabbit Cy3 (Jackson ImmunoResearch

Fig. 7 | Effect of anti-MIP-1α and anti-MIP-1β and role of MIPs in PVR in mice. **a**, **b** Wild type C57Bl/6 mice received anterior chamber injections (3 ul) of anti-MIP-1α (30 μg/ml), anti-MIP-1β (30 μg/ml), or a combination of the two 1 day after intravitreal injection of dispase. At 4 weeks, the eyes were harvested, fixed, embedded, sectioned, and stained with H and E. PVR histology (**a**) and RPE migration (**b**) scores were recorded by trained, masked observers. Shown are mean ± SE, $n = 5–7$ animals/group. Each point represents the average score for 2 trained, independent observers for standard sections from each of 3 or 4 mice in each experimental group. Shown for (**a** and **b**) are mean values ± SE, with p values determined by unpaired one-way ANOVA and the post hoc Tukey test. **c**–**h** Working model for MIP-dependent development of PVR in the dispase model in mice. **c** RPE cells occupy the space between the retina and Bruch's membrane. **d** Upon injury, circulating blood monocytes are released into the wound and differentiate into macrophages. **e** Macrophages elaborate MIP-1α/β, which enables further macrophage migration, disengagement of RPE cells from Bruch's membrane, and migration of RPE cells through the retinal would to the vitreal surface of the retina. (**f**) MIP-1α/β signals kinase-mediated tyrosine phosphorylation of A2, thereby promoting its translocation to the surface of RPE cells, allowing cell surface activation of plasmin (PN) from plasminogen (Plg). **g** Plasmin-bearing, fibroblast-like RPE cells migrate through the retina to the vitreal surface, and (**h**) secrete scar-forming proteins that induce tractional detachment of the retina. Source data for **a** and **b**, are provided as a Source File. Panels **c**-**h** were created with permission by adapting Fig. 1 from Chikafumi Chiba (ref. 6).

Laboratories; 711-165-152, 1:300), donkey anti-goat Alexa 647 (Invitrogen; A21447, 1:100); and donkey anti-rabbit Cy5 (Jackson ImmunoResearch Laboratories; 711-175-152, 1:100).

Murine macrophages

Bone marrow-derived macrophages (BMDMs) were isolated as described[46]. Briefly, fresh marrow was flushed from mouse femurs and tibias under sterile conditions, and cultured for 7 days in complete macrophage medium (Dulbecco's modified Eagle's medium, Gibco #10565) supplemented with 20% L-cell conditioned medium, 10% heat-inactivated fetal bovine serum (FBS, Corning #35-016-CV), 2 mM L-glutamine (Corning #25-005-CL), and 1X penicillin-streptomycin (Corning #30-002-CL). After rinsing twice in PBS (37 °C), adherent BMDMs were harvested by incubation in PBS containing 5 mM EDTA (15 min, 4 °C), detached by gentle scraping, pelleted at 2000 × g (10 min, 4 °C), and resuspended in macrophage medium.

Cytokine and chemokine assays

Retinas (4 per group) were isolated, snap frozen in liquid N_2, and stored in −80 °C. Frozen retinas were homogenized by incubation in radioimmunoprecipitation (RIPA) buffer (50 mM Tris-HCl, pH 7.5, 150 mM NaCl, 1 mM EDTA, 1% NP-40, 1% Na deoxycholate, with phosphatase and protease inhibitor cocktail (Roche PhosStop 04-906-837-001 & cOmplete tablets, mini EDTA-free 04-693-159-001; 250 μl, 4 °C) with agitation. Homogenates were centrifuged (16,000 × g, 20 min, 4 °C), and lysates stored in 50-ul aliquots at −80 °C. Cyto/chemokine screening profiles were performed using a Multi-Analyte ELISArray kit (Qiagen MEM-004A and MEM-009A). For cultured cell chemokine assays, *Anxa2*$^{+/+}$ or *Anxa2*$^{-/-}$ BMDMs (2×10^5 per well) were seeded in 48-well cluster dishes, and post culture medium (100 μl/sample) assayed. MIP-1α and MIP-1β in culture media and tissue homogenates were assayed by ELISA (Qiagen SEM02948A and SEM02949A).

Murine retinal pigment epithelial cells

Two-month-old *Anxa2*$^{+/+}$ and *Anxa2*$^{-/-}$ mice were euthanized by CO_2 inhalation. The eyes are enucleated, dipped in 70% ethanol, and placed in a petri dish containing HEPES buffered Hanks' balanced salt solution (HBSS; Corning #21-021-CV). After removing any extraocular tissue, the eyes are transferred to a tube containing HBSS (2 h, 4 °C, in the dark), and then transferred to a dish containing 2% dispase (Gibco #17105-041) in HBSS (45 min, 37 °C, in a 5% CO_2 incubator). The eyes were then rinsed twice with growth medium (GM; DMEM [Gibco #11965-092], 10% fetal bovine serum [Corning, #35-016-CV], 1X N1 Medium supplement [Sigma, #N6530], 1X GlutaMax-1 [Gibco, #35050-061], 1X MEM Non-Essential Amino Acids [MEM NEAA, Gibco, #11140-050], 125 mg taurine [Sigma T-0625], 10 μg hydrocortisone [Sigma H-0396], 6.5 mg Triiodo-thyronine [Sigma T-5516], 100 U/ml penicillin G, and 0.1 mg/mL streptomycin sulfate [Corning, #30-002-CI])[47]. Next, the corneas were nicked with a #11 blade, and, after making a circumferential cut just below the limbus, the lens was removed, the retina was peeled away from the RPE, and the optic nerve severed. The eyecups were incubated in growth medium (20 min, 5% CO_2, 37 °C), and then cut into 4 quadrants and the RPE sheets teased free with a 30 G needle. RPE sheets from 8 eyes were pooled in a 15-ml centrifuge tube containing growth medium (GM), and centrifuged at 400 g (5 min). The supernatant was discarded, and the pelleted RPE cells gently resuspended in 0.5 ml GM and plated in one well of a 12 well tissue culture plate[47]. The plate was maintained undisturbed for 4–5 days (5% CO_2, 37 °C), after which half of the GM was replaced with fresh medium twice weekly. The cells were split 1:3 at confluency for propagation. Cell identity was verified by cell shape, pigmentation, and staining with RPE-65.

Bone marrow transplantation

Anxa2$^{+/+}$ and *Anxa2*$^{-/-}$ mice received 1200 cGy total body irradiation, and were then immediately rescued with bone marrow (1×10^7 cells in 100 μl saline) from either *Anxa2*$^{LacZ/+}$ or *Anxa2*$^{LacZ/-}$ mice by tail vein injection. Four to five weeks later, the left eye was injected with dispase (0.9 U in 3 μl), and the eyes and lungs harvested at either 48 h or 1 week for analysis of bone marrow cell recruitment.

ARPE-19 culture and migration

Human retinal pigment epithelial cells (ARPE-19; ATCC #CRL-2302; Lot #70004873 or a second ATCC-derived line kindly donated by Dr. Enrique Rodriguez-Boulan at Weill Cornell Medicine) were propagated in Eagle's minimal essential medium (MEM, Corning, #10-022-CV) containing 1% FBS, 1X N1 medium supplement (Sigma, #N6530), 1X GlutaMax-1 (Gibco, #35050-061), 1X MEM Non-Essential Amino Acids (Gibco, #11140-050), 250 mg/L taurine (Sigma T-0625), 20 μg/L hydrocortisone (Sigma H-0396), 0.013 μg/L triiodo-thyronine (Sigma T-5516), 100 U/ml penicillin G, and 0.1 mg/mL streptomycin sulfate (Corning, #30-002-CI)[47]. After three-four weeks, the cells stained strongly positive for RPE-65 and developed pigmented intracellular granules. After several additional weeks in culture, ARPE-19 cells developed evidence of polarity, as demonstrated by transepithelial resistance and expression of the tight junction protein zonulin-1.

For directed migration experiments, ARPE-19 cells, propagated in culture for at least 6–8 weeks under low serum conditions, were seeded on human laminin (Corning #354221, 25 μg/ml, 1 h)-coated, 3 μm pore, Transwell inserts (Costar #3472, 2 × 104 cells/well) positioned within 24-well cluster dishes. Inserts were overlain with hRPE basic medium (100 μl) consisting of MEM, 5% FBS, 100 U/ml penicillin G, and 0.1 mg/mL streptomycin sulfate, while bottom chambers contained basic hRPE media with 5% FBS (500 μl). THP-1 cells (ATCC, #TIB-202) were differentiated by incubation with 20 nM phorbol 12-myristate 13-acetate (PMA, Sigma, #P8139; 3×10^6 cell/ml) in THP-1 medium consisting of RPMI 1640 (Gibco #11875), 10% fetal bovine serum, 100 U/ml penicillin G, and 0.1 mg/mL streptomycin sulfate, 2 mM L-glutamine (Cellgro, #25005CI) in 100-mm dishes[48]. On day 7, the activated, adherent THP-1 cells were washed twice with PBSCM (PBS with 0.9 mM $CaCl_2$ and 0.5 mM $MgCl_2$), harvested, and seeded (2×10^5 per well) in the lower chamber in 5% FBS basic hRPE media (500 μl), and the medium replaced 24 h later with fresh hRPE basal media (5% FCS) to remove unattached THP-1 cells. At the same time, hRPE cells were

seeded (2×10^4 per well) in 5% FBS basic hRPE media (100 μl) on human laminin-coated (Corning #354221, 25 μg/ml, 1 h), 3-μm pore, Transwell inserts (Costar #3472, 2×10^4 cells/well) positioned above the wells of 24-well cluster dishes. For blocking experiments, hRPEs were pre-incubated with test antibodies (4 h, 1 μg/ml) including mouse anti-human A2 IgG1 (BD, #610069, 1 ug/ml), non-immune mouse IgG1 (BD, #550878, 1 ug/ml), goat anti-human MIP-1α (R&D, #AF-270-NA, 1 ug/ml), goat anti-human MIP-1β (R&D, #AF-271-NA, 1 ug/ml,), goat IgG (R&D, #AB-108-C, 1 ug/ml), tranexamic acid or glycine (2 mM, Sigma #857653 and #G7126, respectively, 4 h), and then transferred to THP-1-containing wells. Antibodies or other reagents were added to the top chamber. After 18 h, Transwells were washed twice with cold PBSCM, and fixed with 4%PFA/PBSCM (10 min, 4 °C). Cells were gently removed from the upper surface with cotton swabs, and cells adhering to the under surface stained with 0.05% crystal violet (Sigma, #C-3886; 21 °C, 20 min)[49]. The filters were then washed 4 times, air dried (2 h), and the dye extracted in 125 μl ice cold 100% methanol. The number of migrated cells was estimated by extrapolation of A_{540} values against a standard curve constructed with the same batch of ARPE-19 cells seeded in triplicate in 96-well plates, fixed, stained, and extracted in parallel. For recombinant MIP1α/β stimulation experiments, hRPEs (2×10^4 cells/well) were seeded in 100 μl hRPE basic medium on 3 μm pore Transwell inserts coated with human laminin. Bottom chambers contained 500 μl basic hRPE media with or without 250 ng/ml rhMIP-1α (R&D, #270-LD-010) and/or rhMIP-1β (R&D, #271-BME-010). Migrated ARPE-19 cells were quantified 18 h later, as described.

Assessment of cell surface A2 expression

After 6-8 weeks in culture under low serum conditions, confluent ARPE-19 cells (2×10^7 cells) were passaged (0.25% trypsin-EDTA; Corning, #25-053-CI) and plated in hRPE basic media (2×10^6 cell per 60-mm dish). Two activated THP1/hRPE co-culture 100-mm dishes were also prepared. One day later, fully confluent hRPE cells were washed twice, and incubated with conditioned media or other reagents (18 h). For cell surface biotinylation, the cells were washed twice with ice-cold PBS-CM and incubated twice with sulfo-NHS-SS-biotin (Thermo-Scientific, #21331; 1 mg/ml, 30 min, 4 C, in the dark). The biotinylation reaction was quenched with 50 mM NH_4Cl, and the cells washed again with PBSCM. The samples were lysed (25 mM Tris-HCl, pH 8.0, 1% Triton X-100, 150 mM NaCl, 1 mM EDTA, 1 mM phenylmethylsulfonylfluoride, and Roche protease inhibitor cocktail), and fresh lysate (350–500 μg) incubated overnight with NeutrAvidin Agarose Resin beads (Thermo Scientific, #29200; 50 μl). The beads were washed thrice with lysis buffer, thrice with high salt buffer (50 mM Tris-HCl pH 8.0, 500 mM NaCl), and thrice with low salt buffer (50 mM Tris-HCl pH 8.0). Bound proteins were eluted with SDS sample buffer and resolved on 4 - 20% linear gradient Tris-glycine SDS-PAGE gels (Invitrogen), transferred to 0.2-μm nitrocellulose (Bio Rad), blocked, and incubated with mouse anti-A2 IgG (BD #610069, 1 Greek microg/ml, or Cell Signaling #8235, 1 Greek microg/ml; 18 h, 4 °C), followed by secondary antibodies. For anti-chemokine inhibition studies, goat anti-human MIP-1α and MIP-1β (R&D, #AF-270-NA, 1 Greek microg/ml and #AF-271-NA, 1 ug/ml) or non-immune IgG (R&D, #AB-108-C, 1 ug/ml) were added 4 hours before CM harvesting. A second administration of antibody (1 μg/ml) was provided at the time of treatment with CM.

Antibody development and characterization

Antibodies directed against the N-terminus of human annexin A2 were developed by phage display in collaboration with Pfizer Pharmaceuticals, and expressed as whole IgGs by LakePharma Inc. Human annexin A2 is 98% identical to murine annexin A2, and 100% identical in the first 28 amino acids. Antibody affinity (27-379 nM) and specificity (no reactivity with annexin A1) were assessed by surface plasmon resonance (Bio-Rad Proteon™ XPR36 SPR system) at the High Throughput Screening Resource Center at Rockefeller University (Suppl. Figure 6a). A General Layer Compact (GLC) sensor chip (Bio-Rad, 176-5011) was initialized with air, followed by 50% v/v glycerol in water. The chip was pre-conditioned with 0.5% SDS, 50 mM NaOH and 100 mM HCl (Bio-Rad ProteON RegenerAtion and Conditioning Kit, #1762210), and activated with 1-ethyl-3-(3-dimethyl-aminopropyl) carbodiimide hydrochloride and N-hydroxysulfosuccinimide. Antibodies (10 μg/ml in Na acetate buffer, ProteOn Immobilization Buffer Kit, #1762110) were applied to the chip's 6 channels, and the chip deactivated with ethanolamine to remove excess surface ligand. Antibody interactions with recombinant human annexins A2 and A1 were assessed over a range of concentrations (0, 40, 80, 160, 320, and 640 nM), and the resulting sensorgrams, depicting binding responses versus time, used to derive kinetic rate and equilibrium constants.

Functional activity was assessed by inhibition of plasmin generation as previously described (Suppl. Figure 6b)[50]. Briefly, 96-well plates (black with clear bottom) were coated with 50 ul of 10 ug/ml recombinant human annexin A2 in 100 mM carbonate buffer (pH 9.6, 18 h, 4 °C). After washing with PBSCM, the plate was blocked with PBSCM containing1.5% BSA and 0.05% Tween-20 (1 h, 21 °C), washed (0.05% Tween-20 in PBSCM), and incubated with antibody over a range of concentrations (0.1–50 Greek microg/ml, 1 h, 21 °C). After washing, the plate was incubated with 170 nM human Glu-plasminogen (1 h, 4 °C), placed on ice and washed prior to addition of 40 nM tPA and 125 μM plasmin substrate (D-Val-Leu-Lys aminofluoromethyl coumarin in 0.2% BSA in PBSCM). The fluorescent signal, a reflection of plasmin activity, was recorded at excitation 400 nm and emission 505 nm at 37 °C for 1 h at 3 min intervals. The rate of plasmin generation was calculated as the slope of the plot of relative fluorescence units versus time squared (RFU/min squared).

Human Subjects

According to Weill Cornell Medicine Institutional Review Board-approved protocol (#1307014116R002), and with written informed consent of all protocol participants, fragments of preretinal membranes removed at surgery, were deidentified, placed on MF-Millipore filters, and fixed with 2% paraformaldehyde (10 min, 21 °C). The samples were stained with mouse anti-CD68 (DAKO, M0876) or mouse anti-RPE65 with rabbit anti-A2 (Cell Signaling, 8235S), followed by donkey anti-mouse Alexa 488 (A21202, 1:500, Invitrogen) or donkey anti-rabbit CY3 (711-165-152, 1:300, Jackson ImmunoResearch). After coverslipping, images were acquired with a Nikon 80i microscope 20X or confocal Zeiss LSM 510.

Statistics and Reproducibility

Data are presented as mean ± SEM. Parametric methods (one-way Student's t test or ANOVA with Tukey's post hoc test) were used for non-categorical data sets. All experiments were conducted with the inclusion of appropriate controls. Sample sizes were chosen based on the results of preliminary experiments, and data were excluded only if obvious technical errors were noted. For all animal studies, mice were randomized into experimental groups and tissue samples were analyzed in a double blind fashion with 2-4 independent, trained observers.

Reporting summary

Further information on research design is available in the Nature Portfolio Reporting Summary linked to this article.

Data availability

All data supporting the findings described herein are available in the paper, in the associated Supplementary Information, or from the corresponding author upon request. Source data for this paper are also provided in with this paper. Source data are provided with this paper.

References

1. Morescalchi, F. et al. Proliferative vitreoretinopathy after eye injuries: an overexpression of growth factors and cytokines leading to a retinal keloid. *Mediators Inflamm.* **2013**, 1–12 (2013).
2. Pennock, S., Haddock, L. J., Eliott, D., Mukai, S. & Kazlauskas, A. Is neutralizing vitreal growth factors a viable strategy to prevent proliferative vitreoretinopathy? *Prog. Retin Eye Res.* **40**, 16–34 (2014).
3. Pastor, J. C., Rodriguez de la Rua, E. & Martin, F. Proliferative vitreoretinopathy: risk factors and pathobiology. *Prog. Retinal Eye Res.* **21**, 127–144 (2002).
4. Kwon, O. W., Song, J. H. & Roh, M. I. Retinal detachment and proliferative vitreoretinopathy. *Dev. Ophthalmol.* **55**, 154–162 (2016).
5. Idrees, S., Sridhar, J. & Kuriyan, A. E. Proliferative vitreoretinopathy: a review. *Int Ophthalmol. Clin.* **59**, 221–240 (2019).
6. Chiba, C. The retinal pigment epithelium: an important player of retinal disorders and regeneration. *Exp. Eye Res.* **123**, 107–114 (2014).
7. Kalluri, R. & Weinberg, R. A. The basics of epithelial-mesenchymal transition. *J. Clin. Invest* **119**, 1420–1428 (2009).
8. Duffield, J. S., Lupher, M., Thannicki, V. J. & Wynn, T. A. Host responses in tissue repair and fibrosis. *Annu Rev. Pathol. Mech. Dis.* **8**, 241–276 (2013).
9. Tamiya, S. & Kaplan, H. J. Role of epithelial-mesenchymal transition in proliferative vitreoretinopathy. *Exp. Eye Res.* **142**, 26–31 (2015).
10. Pastor, J. C. et al. Proliferative vitreoretinopathy: a new concept of disease pathogenesis and practical consequences. *Prog. Retin Eye Res.* **51**, 125–155 (2016).
11. Garweg, J. G., Tappeiner, C. & Halberstadt, M. Pathophysiology of proliferative vitreoretinopathy in retinal detachment. *Surv. Ophthalmol.* **58**, 321–329 (2013).
12. Wickham, L. & Charteris, D. G. Glial cell changes of the human retina in proliferative vitreoretinopathy. *Dev. Ophthalmol.* **44**, 37–45 (2009).
13. Awad, M. et al. Delayed presentation and increased prevalence of proliferative vitreoretinopathy for primary rhegmatogenous retinal detachments presenting during the COVID-19 pandemic lockdown. *Eye* **35**, 1282–1283 (2021).
14. Weichel, E. D. & Colyer, M. H. Combat ocular trauma and systemic injury. *Curr. Opin. Ophthalmol.* **19**, 519–525 (2008).
15. Nyugen, Q. D., Kruger, E. F., Kim, A. J., Lashkari, M. H. & Lashkari, K. Combat eye trauma: intraocular foreign body injuries during the Iran-Iraq War (1980-1988). *Int Ophthalmol. Clin.* **42**, 167–177 (2002).
16. Ryan S. J., Sadda S. R., Hinton D. R. *Pathogenesis of Proliferative Vitreoretinopathy* In: *Retina* (eds Ryan SJ, Schachat A, Wilkinson CC, Hinton DR, Sadda SR, Wiedemann P). 5th edn. Elsevier (2012).
17. Hajjar, K. A., Jacovina, A. T. & Chacko, J. An endothelial cell receptor for plasminogen/tissue plasminogen activator: I. Identity with annexin II. *J. Biol. Chem.* **269**, 21191–21197 (1994).
18. Brownstein, C. et al. Annexin II mediates plasminogen-dependent matrix invasion by human monocytes: enhanced expression by macrophages. *Blood* **103**, 317–324 (2004).
19. Law, A. L. et al. Annexin A2 regulates phagocytosis of photoreceptor outer segments in the mouse retina. *Mol. Biol. Cell* **20**, 3896–3904 (2009).
20. Luo, M. & Hajjar, K. A. Annexin A2 system in human biology: cell surface and beyond. *Sem. Thromb. Hemost.* **39**, 338–346 (2013).
21. Deora, A. B., Kreitzer, G., Jacovina, A. T. & Hajjar, K. A. An annexin 2 phosphorylation switch mediates its p11-dependent translocation to the cell surface. *J. Biol. Chem.* **279**, 43411–43418 (2004).
22. Valapala, M., Maji, S., Borejdo, J. & Vishwanatha, J. K. Cell surface translocation of annexin A2 facilitates glutamate-induced extracellular proteolysis. *J. Biol. Chem.* **289**, 15915–15926 (2014).
23. Peterson, E. A., Sutherland, M. R., Nesheim, M. E. & Pryzdial, E. L. Thrombin induces endothelial cell-surface exposure of the plasminogen receptor annexin 2. *J. Cell Sci.* **116**, 2399–2408 (2003).
24. Huang, B. et al. Hypoxia-inducible factor-1 drives annexin A2 system-mediated perivascular fibrin clearance in oxygen-induced retinopathy in mice. *Blood* **118**, 2918–2929 (2011).
25. Krishnan, S. et al. Annexin II-mediated plasmin generation activates TGF-·3 during epithelial-mesenchymal transformation in the developing avian heart. *Dev. Biol.* **265**, 140–154 (2004).
26. Canto Soler, M. V., Gallo, J. E., Dodds, R. A. & Suburo, A. M. A mouse model of proliferative vitreoretinopathy induced by dispase. *Exp. Eye Res.* **75**, 491–504 (2002).
27. Agrawal, R. N. et al. In vivo models of proliferative vitreoretinopathy. *Nat. Protoc.* **2**, 67–77 (2007).
28. Ling, Q. et al. Annexin II regulates fibrin homeostasis and neoangiogenesis in vivo. *J. Clin. Invest* **113**, 38–48 (2004).
29. Banerjee, S. et al. Multiplex bead analysis of vitreous humor of patients with vitreoretinal disorders. *Inv Ophthalmol. Vis. Sci.* **48**, 2203–2207 (2007).
30. Ricker, L. J. A. G. et al. Prediction of proliferative vitreoretinopathy after retinal detachent surgery; potential of biomarker profiling. *Am. J. Ophthalmol.* **154**, 347–354 (2012).
31. Wladis, E. J., Falk, N. S., Iglesias, B. V., Beer, P. M. & Gosselin, E. J. Analysis of the molecular biologic milieu of the vitreous in proliferative retinopathy. *Retina* **33**, 807–811 (2013).
32. Davatelis, G. et al. Cloning and characterization of a cDNA for murine inflammatory protein (MIP), a novel monokine with inflammatory and chemokinetic properties. *J. Exp. Med.* **167**, 1939–1944 (1988).
33. Charo, I. F. & Ransohoff, R. M. The many roles of chemokines and chemokine receptors in inflammation. *N. Engl. J. Med.* **354**, 610–621 (2006).
34. Viola, A. & Luster, A. D. Chemokines and their receptors: drug targets in immunity and inflammation. *Ann. Rev. Pharm. Toxicol.* **48**, 171–197 (2008).
35. Maurer, M. & von Stebut, E. Macrophage inflammatory protein-1. *Int J. Biochem Cell Biol.* **36**, 1882–1886 (2004).
36. Sherry, B. et al. Resolution of the two components of macrophage inflammatory protein 1, and cloning and characterization of one of those components macrophage inflammatory protein 1beta. *J. Exp. Med.* **168**, 2251–2259 (1988).
37. Dallacasagrande, V., Liu, W., Almeida, D., Luo, M. & Hajjar, K. A. Blockade of annexin A2 prevents early microvasculopathy in murine models of diabetic vasculopathy. *Invest Ophthalmol. Vis. Sci.* **64**, 33–44 (2023).
38. Ploplis, V. A., French, E. L., Carmeliet, P., Collen, D. & Plow, E. F. Plasminogen deficiency differentially affects recruitment of inflammatory cell populations in mice. *Blood* **91**, 2005–2009 (1998).
39. Silva, L. M. et al. Plasmin-mediated fibrinolysis enables macrophage migration in a murine model of inflammation. *Blood* **134**, 291–301 (2019).
40. Das, R., Burke, T. & Plow, E. F. Histone H2B as a functionally important plasminogen receptor on macrophages. *Blood* **110**, 3763–3772 (2007).
41. Miles, L. A. et al. Deficiency of plasminogen receptor, Plg-RKT, causes defects in plasminogen binding and inflammatory macrophage recruitment in vivo. *J. Thromb. Haemost.* **15**, 155–162 (2017).
42. Falcone, D. J., Borth, W., Faisal Khan, K. M. & Hajjar, K. A. Plasminogen-mediated matrix invasion and degradation by macrophages is dependent on surface expression of annexin II. *Blood* **97**, 777–784 (2001).
43. Booij, J. C., Baas, D. C., Beisekeeva, J., Gorgels, T. G. M. F. & Bergen, A. A. B. The dynamic nature of Bruch's membrane. *Prog. Retin Eye Res.* **29**, 1–18 (2010).
44. Das, A., Frank, R. N., Zhang, N. L. & Turczyn, T. J. Ultrastructural localization of extracellular matrix components in human retinal vessels and Bruch's membrane. *Arch. Ophthal* **108**, 421–429 (1990).

45. Plow, E. F. & Plow, J. H. The functions of plasminogen in cardiovascular disease. *Trends Cardiovasc Med*. **14**, 180–186 (2004).
46. Shi, S. & Ehrt, S. Dihydrolipoamide acyltransferase is critical for *Mycobacterium tuberculosis* pathogenesis. *Infect. Immun.* **74**, 56–63 (2006).
47. Fernandez-Godino, R., Garland, D. L. & Pierce, E. A. Isolation, culturing and characterization of primary mouse RPE cells. *Nat. Protoc.* **11**, 1206–1218 (2016).
48. Swisher, J. F. A., Burton, N., Bacot, S. M., Vogel, S. N. & Feldman, G. M. Annexin A2 tetramer activates human and murine macrophages through TLR4. *Blood* **115**, 549–558 (2010).
49. Feoktistova M., Geserick P., Leverkus M. Crystal violet assay for determining viability of cultured cells. *Cold. Spring Harb. Protoc.* **2016**, https://doi.org/10.1101/pdb.prot087379 (2016).
50. Cesarman, G. M., Guevara, C. A. & Hajjar, K. A. An endothelial cell receptor for plasminogen/tissue plasminogen activator: II. Annexin II-mediated enhancement of t-PA-dependent plasminogen activation. *J. Biol. Chem.* **269**, 21198–21203 (1994).

Acknowledgements

Support to KAH from the Centers for Therapeutic Innovation (Pfizer Inc.), the Diabetes and Obesity Biologics Science Forum Award (Novo-Nordisk), the Daedalus Fund for Innovation at Weill Cornell Medicine, the U.S. Army Medical Research and Materiel Command (Grants #W81XWH1410507 and #W81XWH2110390), and the Belfer Diabetes Fund at Weill Cornell Medicine, and support to DJD from Research to Prevent Blindness, Inc. are gratefully acknowledged.

Author contributions

M.L., D.A., V.D., and N.H. performed experimental studies. D.D. provided advice on experimental design. S.K. and M.G. procured human samples. K.H. designed the experiments, analyzed the data, and wrote the manuscript.

Competing interests

The authors declare no competing interests.

Additional information

Supplementary information The online version contains supplementary material available at https://doi.org/10.1038/s41467-024-52675-x.

Correspondence and requests for materials should be addressed to Katherine A. Hajjar.

Peer review information *Nature Communications* thanks Sonia Oliani, Jeremy Lavine and the other anonymous reviewer(s) for their contribution to the peer review of this work. A peer review file is available.

Reprints and permissions information is available at http://www.nature.com/reprints

Publisher's note Springer Nature remains neutral with regard to jurisdictional claims in published maps and institutional affiliations.

Open Access This article is licensed under a Creative Commons Attribution-NonCommercial-NoDerivatives 4.0 International License, which permits any non-commercial use, sharing, distribution and reproduction in any medium or format, as long as you give appropriate credit to the original author(s) and the source, provide a link to the Creative Commons licence, and indicate if you modified the licensed material. You do not have permission under this licence to share adapted material derived from this article or parts of it. The images or other third party material in this article are included in the article's Creative Commons licence, unless indicated otherwise in a credit line to the material. If material is not included in the article's Creative Commons licence and your intended use is not permitted by statutory regulation or exceeds the permitted use, you will need to obtain permission directly from the copyright holder. To view a copy of this licence, visit http://creativecommons.org/licenses/by-nc-nd/4.0/.

© The Author(s) 2024